Spectral investigation of a large-area 2D silicon photonic crystal for mid-IR radiation

L. Prodan[a], P. Gross[a], L. Kuipers[b,c] and K-J Boller[a]

a. Laser Physics and nonlinear Optics group, Department of Science & Technology, University of Twente, P.O. Box 217, 7500 AE Enschede, The Netherlands
b. Optical Techniques Group, Department of Science & Technology, and MESA$^+$ Research Institute, University of Twente, P.O. Box 217, 7500 AE Enschede, The Netherlands
c. Center for Nanophotonics, FOM-Institute for Atomic and Molecular Physics AMOLF, Kruislaan 407, 1098 SJ Amsterdam, The Netherlands

Abstract

A two-dimensional silicon photonic crystal, which is designed to provide a modified dispersion for photon energies of less than half of the electronic band gap of silicon, and which has been fabricated by laser interference lithography, is studied by angular dependent infrared reflectivity measurements. The resonance features, which we observe in the polarized reflectivity spectra, and which arise from resonant coupling of the infrared radiation to the leaky modes, are used to complement photonic band structure calculations to reveal the complete band structure including bandgaps. We also present conclusions on the quality factor of the photonic crystal fabricated by laser interference lithography.

1. Introduction

Photonic crystals (PhCs) are composite materials, where a large, periodic variation of the dielectric function leads to a dramatic change of the propagation properties of light [1]. These crystals can be designed and manufactured to offer specific propagation properties, as desired to achieve e.g., control of spontaneous emission [2], localization of light [3], or

propagation along arbitrary paths [4]. Besides their remarkable linear properties, out of which the above mentioned possibilities arise, such crystals also promise to possess interesting nonlinear properties, many of which are based on altering the index of refraction through the third order optical nonlinearity, $\chi^{(3)}$, and which can lead to the possibility of tuning the transmission wavelength [5, 6] or rapidly switching the transmission of PhCs [7], or designing the spatial and temporal shape of a propagating pulse. The latter can be used to create spatial or temporal solitons, or the combination of both, which often is termed light bullets [8, 9].

However, despite the high potential, the nonlinear properties of PhCs are by far less well investigated and understood than the linear properties. Previous demonstrations of third-order nonlinear effects in PhCs have been dominantly accompanied by unwanted linear (absorption) and resonant third-order nonlinear effects (two-photon losses), which make the observation of the aimed effects difficult. A first step towards the application of PhCs to nonlinear propagation effects would be the transition to the infrared spectral region. Under such circumstances, i.e., when shining light of photon energies less than half the electronic bandgap of Si (1.1 eV, corresponding to a wavelength of 2.1 μm) onto a PhC with a designed dispersion for MIR propagation, two-photon losses will be strongly reduced, the residual material effects could thus be neglected, and the unaltered properties of the structure could be studied.

Leonard and colleagues have demonstrated band-edge tuning using macroporous silicon, where the near-infrared wavelength of 1.9 μm used to probe the PhC modes helped avoiding linear absorption [6], but where the photon energy was still high enough to allow two-photon absorption. A designed dispersion in the mid-infrared spectral region,

as would be desirable for the unaltered observation of third-order nonlinear effects, has not been demonstrated until today, despite the anticipated advantages when using MIR light, and despite the propagation properties of visible and near-infrared light with frequencies relevant for telecommunication being designed and realized almost routinely.

Here, we present the first, linear characterization of a PhC, which has been designed to enable the intended nonlinear experiments, and which has been fabricated using laser interference lithography (LIL). In this contribution, we determine the energy against wave vector dispersion curves in the range from 1.9 to 2.8 μm by means of reflectance spectroscopy at oblique incidence [10]. By recording the resonance spectra for a number of angles of incidence, particular points of the photonic band structure can be probed, and the dispersion curves of the leaky modes are mapped. We determine the quality factors of the PhC from the bandwidth of the observed resonance features, which is, to the authors' knowledge, the first report about the quality factors of a photonic crystal sample manufactured using LIL. Finally, we use the experimentally obtained data to reconstruct the band structure and verify the existence of a bandgap and of the dispersion required for nonlinear experiments in the desired MIR frequency region.

2. Sample design and preparation

Recently, we have designed a photonic crystal such that it should enable the study of nonlinear effects in the desired MIR wavelength range. Specifically, it should offer the possibility to generate both spatial and temporal solitons by exploiting the third-order nonlinear Kerr effect. The generation of such spatio-temporal Kerr-solitons or light bullets has been investigated theoretically [11]. For this purpose, several requirements

must be fulfilled: first, the material in which the light propagates needs to show a sufficiently high *positive* Kerr-coefficient, such that diffraction can be balanced by Kerr-self-focusing. Furthermore, for spatial solitons to form, the medium is required to have 2D or slab geometry, because in 3D or bulk media Kerr-self-focusing is believed to lead to transverse instabilities and eventually to beam break-up [12]. Second, a temporal soliton can form due to the positive Kerr-effect, if it travels through a medium with *anomalous* dispersion [13], which can be realized, e.g., in a PhC in close vicinity to a photonic bandgap, i.e., to a frequency interval within which the propagation of light is not possible. In summary, in order to investigate the formation of spatio-temporal Kerr-solitons, a PhC slab of highly Kerr-nonlinear material is required, which shows anomalous dispersion in the MIR spectral region around 2.6 μm.

The PhC designed for this purpose is based on silicon, which offers a high, positive Kerr-nonlinearity [14], and which has an electronic bandgap energy of 1.1 eV, such that illumination with light of a wavelength longer than 2.1 μm should enable experiments with strongly reduced two-photon absorption. The structure is sketched schematically in the upper left graph of Fig. 1. It is based on a photonic crystal slab design, i.e., a 0.5-μm thick film of silicon on a 3-μm thick SiO_2 layer (silicon on insulator, SOI), which separates the waveguide slab from the underlying Si wafer (not shown in Fig. 1). In such a PhC slab, standard waveguiding confines the light to the PhC plane with a higher index of refraction, i.e., to the silicon layer with $n \approx 3.4$ @ $\lambda = 2.6$ μm (compared to SiO_2 with $n \approx 1.4$ on one side and to air on the other side). The dispersion of in-plane wave vectors is determined by periodic refractive index modulation in the silicon plane. Previoulsy, we have calculated, that a square lattice array of air holes with a diameter of around 0.7 μm

and with a lattice constant of 1 μm should offer the required anomalous dispersion for wavelengths around 2.6 μm. The upper right part of Fig. 1 shows the irreducible Brillouin zone (IBZ) corresponding to this square lattice with the standard notation of the high-symmetry points, Γ, X, and M.

The crystal has been fabricated with LIL [15], a novel technique allowing the production of 2D PhCs of large area and of high periodicity. In order not to alter the properties of the planar waveguide, the etching process has been carefully controlled, such that the holes do not penetrate the SiO_2 layer. The latter has been verified with a scanning electron microscope (SEM) image of the fabricated structure. A second SEM image, which is shown in the lower part of Fig. 1, has been used to verify the 1-μm lattice constant of the square lattice and the high periodicity within the whole 1×1 cm^2 surface of the PhC. We believe, that this exceptionally large surface of the PhC is of particular advantage for the study presented in the following, because the result of a single measurement, where a large portion of the PhC is illuminated simultaneously, is equivalent to an average over a number of measurements over a smaller surface.

3. Experimental setup

The dispersion of the photonic crystal slab is probed by angle- and wavelength-resolved reflectivity measurements. This technique is based on the observation of resonant coupling, when the in-plane component of the incident wavevector matches the wavevector of the photonic bands, and has been applied to PhC slabs earlier [16-19]. Because only the projection of the wavevector can be coupled to the PhC modes, this coupled wavevector is reduced with respect to the wavevector of the light in surrounding

air by a factor sin(θ), where θ is the angle of incidence. Thus, the wavevector does not match the dispersion of the guided modes, which excludes to directly probe the dispersion of guided modes via simple reflection measurements. Rather one expects a coupling only to the leaky (or quasi-guided) modes. In the work described in Ref. 16, a high-index prism has been used to increase the range of accessible energy-wavevector combinations. In our work, we follow a different and less involved approach where the dispersion of the leaky modes is probed to and the band structure of the guided modes is obtained by extrapolation [17].

Preliminary calculations [20] have shown, that for a mapping of the dispersion curves of the leaky modes of our photonic structure, we require a light source that covers the range of photon energies from 0.44 to 0.65 eV, i.e., the wavelength range from 1.9 to 2.8 μm. Additionally, to provide the according wave vector range, the angle of incidence, θ, must be adjustable from 10° to 70°. The divergence of the incident beam is then the limiting factor for the precision: a distribution over a range of angles of incidence will result in a distribution over a range of projected wavevectors and will thus ultimately limit the resolution, with which the coupled wavevector can be determined, and thus the contrast with which spectral features can appear in the reflectivity spectra. Furthermore, the cross section of the beam should be adapted to evenly illuminate a large portion of the PhC structure, such that a single measurement represents the equivalent of averaging over a wide surface area and thus enhance the obtainable signal-to-noise ratio.

To realize a light source with a small beam divergence and tunable spectral range, we employ a broad-bandwidth light source and select appropriate beam shaping, wavelength-selection and polarization optics. The resulting setup is shown schematically in Fig. 3. As

a broad-bandwidth light source, we use a 250 W quartz tungsten halogen (QTH) lamp (Oriel 66995), driven by a stabilized current supply. This white-light source emits a spectral power of more than 3 mW/nm over the desired wavelength range from 1.9 to 2.8 μm. The white light is spectrally filtered using a 300-mm monochromator (Hilger and Watts) with a grating of 750 lines/mm and with blazing for MIR wavelengths. For an efficient throughput, the filament of the QTH bulb is directly imaged onto the entrance slit of the monochromator using a CaF lens with a focal length of 300 mm, a diameter of 50 mm, and an NA chosen to match the acceptance angle of the monochromator. Entrance and exit slits of the monochromator are both set to a width of 1 mm. With a lens of 150 mm focal length and 25 mm diameter, the light emerging from the monochromator is collected and focused onto a slit with 5 mm width. The slit is then imaged onto the PhC using another lens of 500 mm focal length and a pinhole to remove off-axis stray light. Using a wire-grid polarizer, the polarization is chosen to be either parallel or perpendicular to the plane of reflection, i.e., we choose either transversal-electric (TE) or transversal-magnetic (TM) polarized light. Finally, a high-pass optical filter is used to remove light transmitted through the monochromator in higher order.

With this experimental setup, we generate a wavelength tunable mid-IR light beam, which illuminates the PC sample with the following characteristics: the power in front of the sample is approximately 2 nW, with a spectral bandwidth of 5 nm. the beam divergence is estimated to be 3°, which translates into a wavevector error ranging from less than 30% for the smallest angle of incidence, $\theta = 10°$, to less than 2% for $\theta = 70°$. The beam cross section is of rectangular shape with 2 mm by 5 mm, such that, even at high angle of incidence (up to 70°) the projection of the beam cross section is entirely

within the 100 mm^2 area of the sample. This represents a compromise between the wave vector resolution, the spectral resolution, and the signal-to-noise ratio. Narrowing the monochromator slit width, for example, would improve the spectral resolution, but it would also increase the beam divergence and thus disimprove the wave vector resolution, and it would decrease the available power and thus disimprove the signal-to-noise ratio.

The sample is mounted on a rotation stage and rotated around the surface normal, such that the direction of the in-plane wave vector of the incident light, i.e., the projection of the wave vector on the sample surface, is along one of the two symmetry directions Γ–M and Γ–X of the quadratic lattice, i.e. along the directions connecting the symmetry points Γ and M, and Γ and X, respectively. The desired orientation is verified by inspecting the mounted sample with a microscope. A second rotation stage allows the variation of the angle of incidence θ, as required for changing the in-plane component of the incident wavevector (compare Fig. 2).

The light reflected off the PhC surface is weak, of only nW power level, and it is in a spectral region where detectors with low noise and high quantum efficiency are not readily available. Nevertheless, even small changes in reflectivity can indicate coupling to a leaky mode. Therefore, to enable a high signal-to-noise ratio, a sensitive MIR detector is combined with a powerful and low-noise amplifier as follows. After reflection off the surface of the sample, the light passes a rotating-disc optical chopper with the chopping frequency set to 3.5 kHz, and is projected using a lens of 100 mm focal length on the detector. As a detector for the MIR radiation, a photoconductive PbS detector is used (OEC GmbH, model A5-0-3), which is carefully protected from surrounding light as well as from stray light originating from the white-light QTH source. To maximize

detector efficiency, a bias voltage of 110 V is applied. For a high signal-to-noise ratio, a differential pre-amplifier is employed, followed by an integrating amplifier, which, by eliminating the DC component of the signal, ensures that the differential amplifier operates in the linear regime. The circuit is designed similar to the one described in Ref. 21. The amplified detector signal is processed using a lock-in amplifier (Princeton Applied Research Corp., Model 129A). The described detection scheme enables a signal-to-noise ratio of 25 at nW power level in the MIR spectral region and is thus suitable to record even weak changes in reflectivity from the PhC surface.

4. Results and discussion

4.1 Specular reflectivity spectra

Specular reflectivity spectra are obtained along the Γ–M symmetry direction, and along the Γ–X symmetry direction for two perpendicular polarizations of incident light, and for angles of incidence varying between $\theta = 10°$ and 70°. In Fig. 4, the reflectivity of the photonic crystal slab along Γ–M symmetry direction is displayed as a function of wavelength by the black curves, for the two cases when the light was TE polarized (in plane of reflection, Fig. 4a), and when the light was TM polarized (perpendicular to the plane of reflection, Fig. 4b). In both figures, the angle of incidence, θ, increases from bottom ($\theta = 10°$) to top ($\theta = 70°$).

Both sets of spectra show sharp features superimposed on a background, which originates from residual light sources in the room and from stray light of the QTH light source, and which is more dominant for smaller angles of incidence. The sharp features shift in wavelength with the variation of the incidence angle by more than 200 nm. For a better

visibility, the shifting features are connected with a gray line throughout the different spectra. Upon a comparison of the two graphs in Figs. 4a and 4b, it is evident that the spectra recorded for TE polarization clearly differ from those recorded for TM polarization. This shows that modes of different bands are excited either by TE or by TM polarization, and that there is no polarization mixing between TE and TM modes in the PhC slab.

Measurements are also performed along the Γ-X symmetry direction for both polarizations. These spectra are displayed in Figs. 5a (TE polarization) and 5b (TM polarization), and show similar distinct features, which also shift in wavelength, as the angle of incidence is varied. As before, in the case of Γ-M symmetry direction, no polarization mixing is observed.

4.2 Line shapes of observed features

A closer investigation reveals that the features possess different line shapes, such as maxima, minima, and dispersive (asymmetric) forms. Similar asymmetric line shapes have been observed before for the case of one-dimensional structures [22] as well as for two-dimensional square [18] and triangular lattices [19]. In Ref. 23, these dispersive line shapes have been explained by a phase shift of the reflected light when coupling to a leaky mode occurs, and the dependence of the shape of the observed features on the depth of the holes structure could be verified by simulation of the reflectivity. It is evident, however, that these differences in line shape hamper a direct extraction of the center wavelength and the linewidth of the probed leaky modes, which is crucial for the characterization of a PhC. Therefore, to enable an accurate determination of the named

values, we adopt an expression to describe the line shapes, which has been derived in the classical Fano paper from 1961 [24], and which has been used before to describe reflectivity features of photonic crystals [16, 18].

With the energy $E = \hbar\omega$ of the incident photons, the energy of the resonant modes $E_0 = \hbar\omega_0$ with center frequency ω_0, and a linewidth of the resonant mode $\Gamma = \hbar\gamma$, we obtain the reduced energy variable ε in analogy to Eq. 19 of Ref. [24]:

$$\varepsilon = \frac{\hbar\omega - \hbar\omega_0}{1/2\,\hbar\gamma}. \tag{1}$$

The line shape of the features can then be expressed by (compare Eq. 21 of Ref. 24):

$$F(\omega) = F_0 \frac{(q+\varepsilon)^2}{1+\varepsilon^2} = F_0 \cdot \left[1 + \frac{q^2 - 1 + 4q(\omega-\omega_0)/\gamma}{1 + 4(\omega-\omega_0)^2/\gamma^2}\right] \tag{2}$$

Here, F_0 is oscillator strength, while the parameter q may assume values between –1 and +1 and determines the shape of the resonance. The parameter q can be regarded as a coupling parameter of the incident photons to the leaky modes of the PhC (compare Eq. 22 of Ref. 24).

Equation 2 is fitted to the reflectivity features, which can be identified in the experimental data, with the center frequency, the linewidth of the feature, and the *q*-parameter as fitting parameters (two additional fit parameters are an offset and a scaling factor which are not supposed to be of much relevance for the center frequency, linewidth and *q*-parameter fits). In some of the spectra, several, partially overlapping features can be observed. To obtain the center frequencies and linewidths of such features, we apply a linear combination of two or more of such line shapes. We note, however, that such a superposition can be applied only, if the two resonances do not couple, for in that case the

measured line shape may differ substantially from a mere superposition of the two resonance features [25]. As an example, Fig. 6 displays the experimental data obtained for the Γ–X symmetry direction, TM polarization, and for an angle of incidence of 10° (measured points displayed as squares), together with three Fano fits (Eq. 2, solid lines). The fits yield, in this example, features with center wavelengths of 2.06 μm, 2.24 μm, and 2.29 μm (indicated by vertical dotted lines). This example demonstrates the suitability of the Fano function Eq. 2 to describe the measured line shapes in the reflectivity spectra. In the following, we present the results obtained by fitting the described formula to our experimental specular reflectivity spectra, i.e. the bandwidth and the center frequency of the features observed in the spectra.

4.3 Quality factor

The quality factor, Q, of a photonic structure is a measure for the lifetime of a PhC mode and thus of the losses, which can be induced by scattering through the roughness of the surface, but also by irregularities regarding the hole size, hole roundness and hole displacement (i.e. an erratious periodicity). The measurement of Q would thus give a valuable first indication of the quality, i.e. the regularity of a structure that can be expected from this novel manufacturing method LIL. In this contribution, we determine the quality factor Q from the ratio of the center frequency and the linewidth of the measured features, $Q = \frac{\omega_0}{\gamma}$, both being obtained from fitting the Fano lineshape to the measured reflectivity spectra.

The quality factor is calculated for each of the reflectivity features, which could be identified in the measurements presented in Figs. 4 and 5. Most of the values obtained lie

in an interval between about 20 and 70. Only for the Γ-X symmetry direction and TM polarized light, some exceptionally high and probably erroneous values are obtained, which are not considered for the evaluation in order to avoid statistical deviation, such that the resulting mean Q value is more likely to be under-estimated than over-estimated. The Q values obtained for Γ-X symmetry direction yield a mean value of 46 ± 4 for TM polarized light and of 43 ± 3 for TE polarized light. For the second symmetry direction, Γ-M, the mean Q values are 45 ± 4, and 45 ± 5 for TM and TE polarized light, respectively.

The four mean Q values for the two different symmetry directions and the two light polarizations vary hardly, such that we can estimate the quality factor of the 2D PhC to be around 45. This Q factor is about two orders of magnitude lower than what is typically obtained for comparable, defect-free PhC slabs manufactured using other methods, like e.g., electron-beam lithography [5]. The effect is probably intrinsic to the LIL manufacturing process that seems to produce short-range errors in the periodicity (as can also be seen by the slightly irregularly shaped holes in the SEM image). The long range (mm-range) periodicity, on the other hand, is entering the data as well due to the large probe beam diameter. The observed Q-values thus form an upper limit also for long-range periodicity errors, which should be low as compared to other manufacturing methods, because in contrast to those, LIL does not require a displacement of the sample and is thus free of stitching errors [26].

4.4 Leaky modes band structure

From the identified positions of the resonance features, the dispersion of the leaky modes probed by the reflectivity measurements is mapped by plotting the normalized frequency, i.e., the periodicity of the photonic structure over the wavelength of the incident light of the observed resonances as a function of the corresponding normalized wavevector, i.e., the wavevector multiplied by the periodicity over π. The resulting out-of-plane band structure for Γ-M symmetry direction is shown in Fig. 7a for TE polarized light and in Fig 7b for TM polarized light, where the values obtained from the out-of-plane reflectivity experiments are displayed by circles. From left to right, the wavevector increases from 0 to the inverse periodicity in Γ-M direction. The gray line in both graphs represents the light line, i.e. the dispersion of light in air, which indicates the lower limit of the out-of-plane band structure in these graphs. According to the wavelength range chosen for the experiment, the normalized frequency of the probed modes lies around 0.4.

The resonances displayed in Figs. 7a and 7b are then used as an aid to theoretically obtain the complete band structure diagram based on a plane-wave simulation [27]. The simulation is carried out using a periodicity of 1 μm as measured with SEM (Fig. 1), and with the hole diameter as a free parameter, where the best agreement between the simulated band structure and the measured resonances is yielded with a hole diameter of 0.72 μm. In the calculations, the modes are usually referred to as being even or odd with respect to a horizontal symmetry plane. It is known that even modes only couple to TM polarized incident light, while odd modes couple to TE polarized light [17]. In Fig. 7a and 7b the calculated odd and even modes are displayed, respectively, by solid black lines. It can be seen, that a good agreement between measurement and simulation is achieved.

Figure 8 shows the corresponding out-of-plane band structure obtained for the Γ-X symmetry direction, for TE polarized (Fig. 8a) and for TM polarized (Fig. 8b) light. Again, the normalized frequency is plotted as a function of the normalized wavevector, and again, the wavevector increases from left to right until the inverse periodicity in Γ-X direction is reached. As before, the experimental points are displayed as circles, and the corresponding calculated dispersion is given by the solid lines. In the graphs displayed in Fig. 8, the agreement between measured and calculated dispersion is not as clearly visible as it was in Fig. 7. Specifically, for the case of TE polarization (Fig. 8a), the position of the experimental values appear to be at slightly lower frequencies and shorter wavevectors than expected from the calculated dispersion bands; the trend of the band structure, however, is visible also in these graphs.

Generally, we can state that, using experimental reflectivity data to complement the structure parameters of the 2D PhC for the simulations, we have obtained the band structure of the leaky modes.

4.5 Guided modes band structure

Based on the theoretical band structure model combined with data from the reflectivity measurements presented in the previous paragraph, we now can complete the band structure to show the complete dispersion also of the guided modes, i.e., the modes under the light line. Figure 9 shows the so calculated band structure for TE polarized light [27], which is obtained with the same parameter as before, i.e., a periodicity of 1 μm and a hole diameter of 720 nm. In Fig. 9, the normalized frequency is plotted as a function of the normalized wavevector along a path connecting the high-symmetry points Γ-X-M-Γ.

This path is sufficient to show all minima and maxima of all bands [28] and thus allows for the identification of bandgaps, i.e., frequency intervals, which are free of guided modes. The modes are calculated along this path and displayed as solid black lines. The dispersion of light in air, the light line, forms a cone in this graph and is displayed as a solid gray line. In Fig. 9, one can identify several intervals under the light cone, which are free of guided modes. One of these bandgaps is particularly interesting for us, namely the bandgap spanning the frequency range from 0.347 to 0.383, i.e. the wavelength range from 2.61 to 2.88 μm. The named range corresponds to a bandgap for TE polarized light around a wavelength of 2.7 μm and of a width of about 10% of its center wavelength. Close to this bandgap, the PhC guided modes show the strong anomalous dispersion in the MIR spectral range we were aiming at when designing this crystal.

The band structure is completed also for TM polarized light, which is displayed along a path connecting the high-symmetry points Γ-X-M-Γ in Fig. 10. The guided modes for TM polarized light, i.e. the modes lying under the light cone in Fig. 10, also show several gaps, where again one is in the range of interest for us, namely a gap for light frequencies between 0.395 and 0.428, or for wavelengths in the range from 2.34 to 2.53 μm. We thus expect a bandgap for TM polarized light around a wavelength of 2.4 μm and of a width of about 8% of its center wavelength.

For both polarizations, the 2D PhC thus offers a bandgap at photon energies, which are less than half the electronic bandgap of silicon, i.e. at wavelengths longer than 2.1 μm. In the vicinity of this bandgap, the PhC shows a strong anomalous dispersion in a material with a positive Kerr-coefficient, as it is required for spatio-temporal solitons to form. In

conclusion, a prerequisite for performing nonlinear experiments is fulfilled with the fabrication of this PhC.

5. Summary and conclusion

In summary, we have presented the first, linear characterization of a square-lattice photonic crystal slab based on Si. The PhC has been designed to provide strong anomalous dispersion in the MIR wavelength range above 2.1 μm in order to enable the formation of spatio-temporal solitons and study nonlinear effects, and has been fabricated using laser LIL. We have obtained the energy against wave vector dispersion curves in the range from 1.9 to 2.8 μm by means of reflectance spectroscopy at oblique incidence and have, for the first time, determined the quality factors of a PhC sample manufactured using LIL. From our results, it seems that LIL, in comparison with other commonly sed processes, enables the manufacturing of large structures of rather poor short-range quality, but of excellent long (mm-) range periodicity.

Form the angular reflectivity measurements, we have mapped the dispersion curves of the leaky modes and have used the experimentally obtained data to reconstruct the band structure and to verify the existence of several bandgaps. In the vicinity of the bandgaps, a region of anomalous dispersion could be identified as required for nonlinear experiments in the MIR spectral region.

In conclusion, we have designed, manufactured, and verified the dispersion properties of a PhC slab using calculations complemented by specular reflectivity experiments. The highly nonlinear Kerr material with modified dispersion in the MIR should enable us to

perform nonlinear experiments at elevated light intensities, while the nonlinear, i.e. two-photon losses are reduced due to the low photon energies.

Acknowledgements

The authors acknowledge financial support by the Dutch Stichting voor Fundamenteel Onderzoek der Materie (FOM) and the Nederlandse Organisatie voor Wetenschappelijk Onderzoek (NWO). We gratefully thank Prof. Dr. R. Beigang, Dr. C. Bostan and Dr. M.E. Klein for stimulating discussions, and we thank J. Couperus, M. Smithers and the clean room staff of the MESA$^+$ Research Institute for technical support.

References

[1] J. D. Joannopoulos, R. D. Maede, and J. N. Win, *Photonic crystals, molding the flow of light*, Princeton University Press, Princeton, NJ 1995

[2] E.Yablonovitch, Phys. Rev. Lett. **58**, 2059-2062 (1987)

[3] S. John, Phys. Rev. Lett. **58**, 2486 (1987)

[4] S. Fan, J.N. Winn, A. Devenyi, J. C. Chen, R. D. Meade, J. D. Joannopoulos, J. Opt. Soc. Am. B **12**, 1267 (1995)

[5] F. Raineri, C. Cojocaru, R. Raj, P. Monnier, A. Levenson, C. Seassal, X. Letartre, P. Viktorovitch, Opt. Lett. **30**, 64 (2005)

[6] S.W. Leonard, H.M. van Driel, J. Schilling and R.B. Wehrspohn, Phys. Rev. B **66**, 161102(R) (2002)

[7] A. Hache and M. Bourgeois, Appl. Phys. Lett. 77, 4089 (2000)

[8] G. Fibich and B. Ilan, Opt.Lett. **29**, 887 (2004)

[9] H. S. Eisenberg, R. Morandotti, Y. Silberberg, S. Bar-Ad, D. Ross and J. S. Aitchison, Phys. Rev. Lett. **87**, 043902 (2001)

[10] V.N. Astratov, R.M. Stevenson, M.S. Skolnick, D.M. Whittaker, S. Brand, I. Culshaw, T.F. Krauss, R.M. De La Rue, and O.Z. Karimov, IEE Proc. Optoelectron. **145**, 398-402 (1998)

[11] P.M. Goorjian and Y. Silberberg, J.Opt. Soc. Am. B **14**, 3253 (1997)

[12] P.L. Kelly, Phys. Rev. Lett. **15**, 1005 (1965)

[13] L.F. Mollenauer, R.H. Stolen, and J.P. Gordon, Phys. Rev. Lett. **45**, 1095 (1980)

[14] M. Dinu, F. Quochi, and H. Garcia, Appl. Phys. Lett. **82**, 2954 (2003)

[15] L. Prodan, T.G. Euser, H.A.G.M. van Wolferen, C. Bostan, R.M. de Ridder, R. Beigang, K-J Boller and L. Kuipers, Nanotechnology **15**, 639 (2004)

[16] M. Galli, D. Bajoni, M. Belotti, F. Paleari, M. Patrini, G. Guizzetti, D. Gerace, M. Agio, L.C. Andreani, D. Peyrade, and Y. Chen, IEEE Journal on selected areas in communications **23**, 1402 (2005)

[17] L. C. Andreani and M. Agio, IEEE J. Quantum Electron. **38**, 891 (2002)

[18] V. Pacradouni, W. J. Mandeville, A. R. Cowan, P. Paddon, Jeff F. Young, S. R. Johnson, Phys. Rev. B **62**, 4204 (2000)

[19] V. Astratov, D.M. Whittaker, I.S. Culshaw, R.M. Stevenson, M.S. Skolnick, T.F. Krauss and R.M. De La Rue, Phys. Rev. B **60**, R16255 (1999)

[20] The calculations were carried out using a 30-day trial version of the DiffractMOD^{TM} software packet. DiffractMOD^{TM} is a registered trademark of the Rsoft Design Group Inc.

[21] T. Berger and E. Brookner, Applied Optics **6**, 4204 (2001)

[22] D. Peyrade, Y. Chen, A. Talneanu, M. Patrini, M. Galli, F. Marabelli, M. Agio, L.C. Andreani, E. Silberstein, P. Lalanne, Microelectronic Engineering **61-62**, 529 (2002)

[23] V. N. Astratov, I. S. Culshaw, R. M.Stevenson, D. M.Whittaker, M. S. Skolnick, T. F. Krauss, and R. M. De La Rue, J. Lightwave Techn. **17**, 2050 (1999)

[24] U. Fano, Phys. Rev. **124**, 1866 (1961)

[25] F. H. Mies, Phys. Rev. **175**, 164 (1968)

[26] V. Berger, O. Gauthier-Lafaye, and E. Costard, El. Lett. **33**, 425 (1997)

[27] S. G. Johnson and J. D. Joannopoulos, Opt. Expr. **8**, 173 (2001)

[28] T. Ochiai and K. Sakoda, Phys. Rev. B **64**, 045108 (2001)

Figure 1

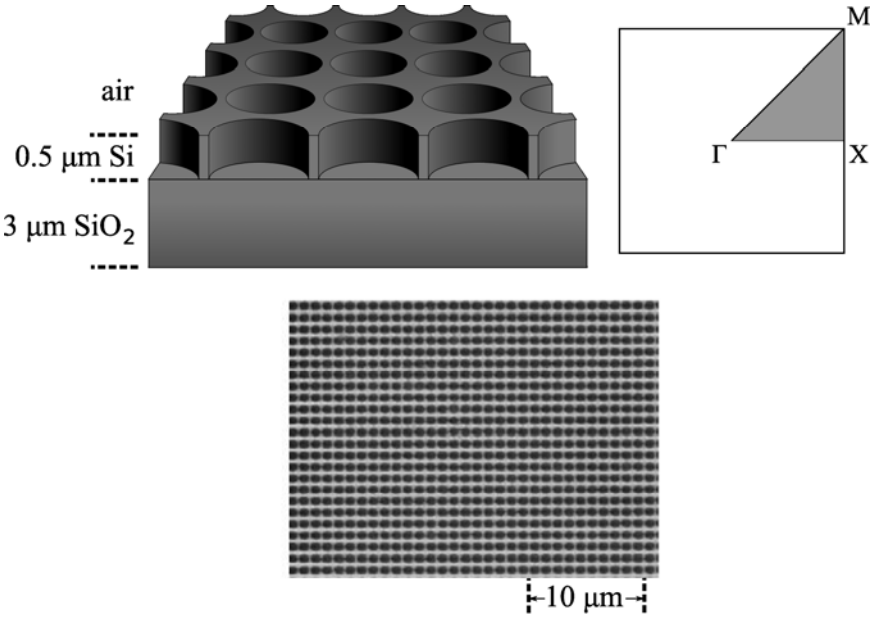

Upper left: schematic of the 2D photonic crystal consisting of a square lattice of holes in silicon. Upper right: Corresponding irreducible Brillouin zone with the high-symmetry points Γ, X and M. Lower: SEM micrograph of the photonic crystal, top view.

Figure 2

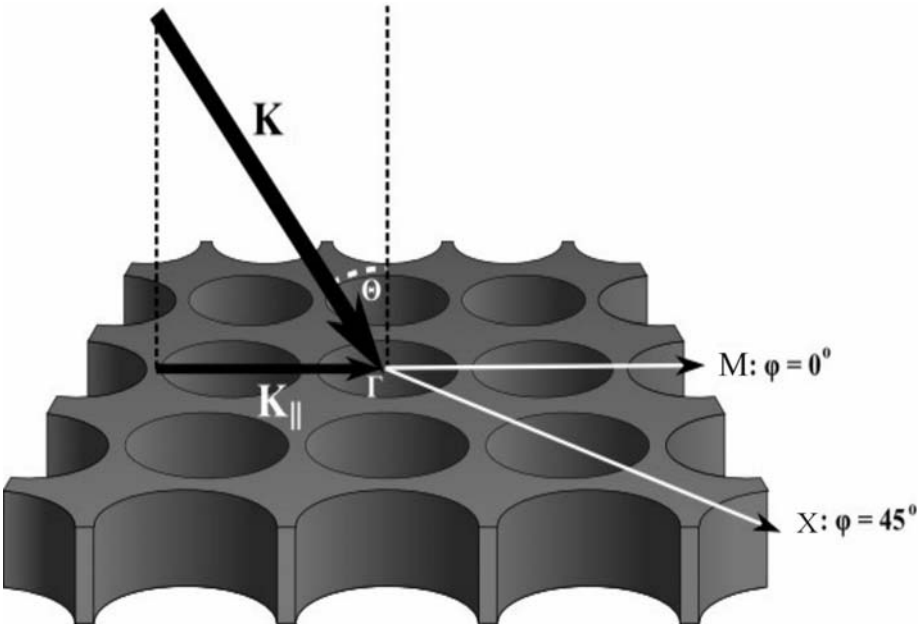

Schematic representation of the K vector of the incident light projected on the plane of the slab. The in-plane wave vector of the incident light is K_{II} and is determined by the angle of incidence light θ. The angle between the Γ–X and Γ–M crystal symmetry direction is 45°.

Figure 3

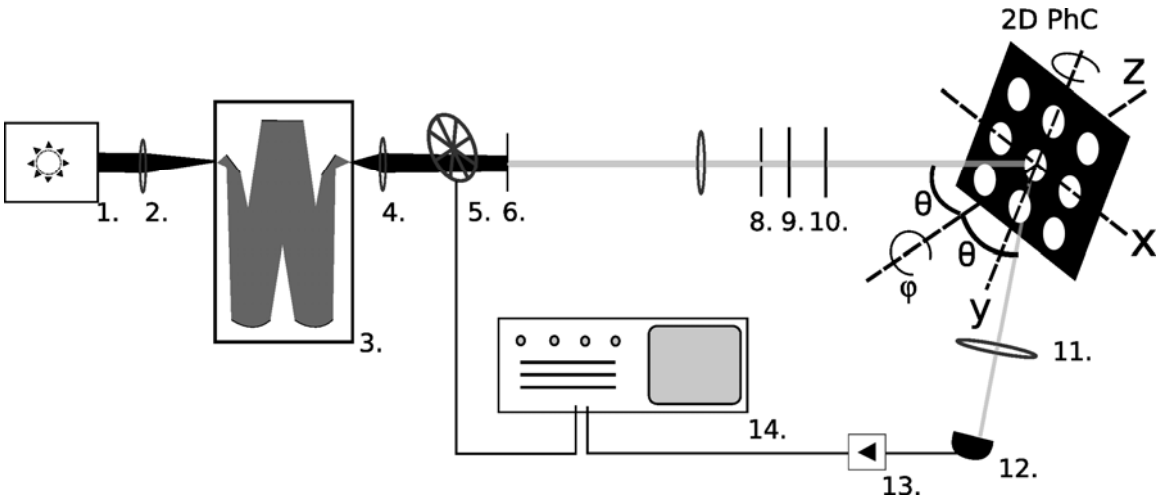

Experimental setup for specular reflectivity measurements. The individual components are: 1, QTH light source; 2, lens; 3, monochromator; 4, lens; 5, optical chopper; 6, slit; 7, lens; 8, pinhole; 9, low-pass filter; 10, polarizer; 11, lens; 12, detector; 13, amplifier; 14, lock-in amplifier.

Figure 4

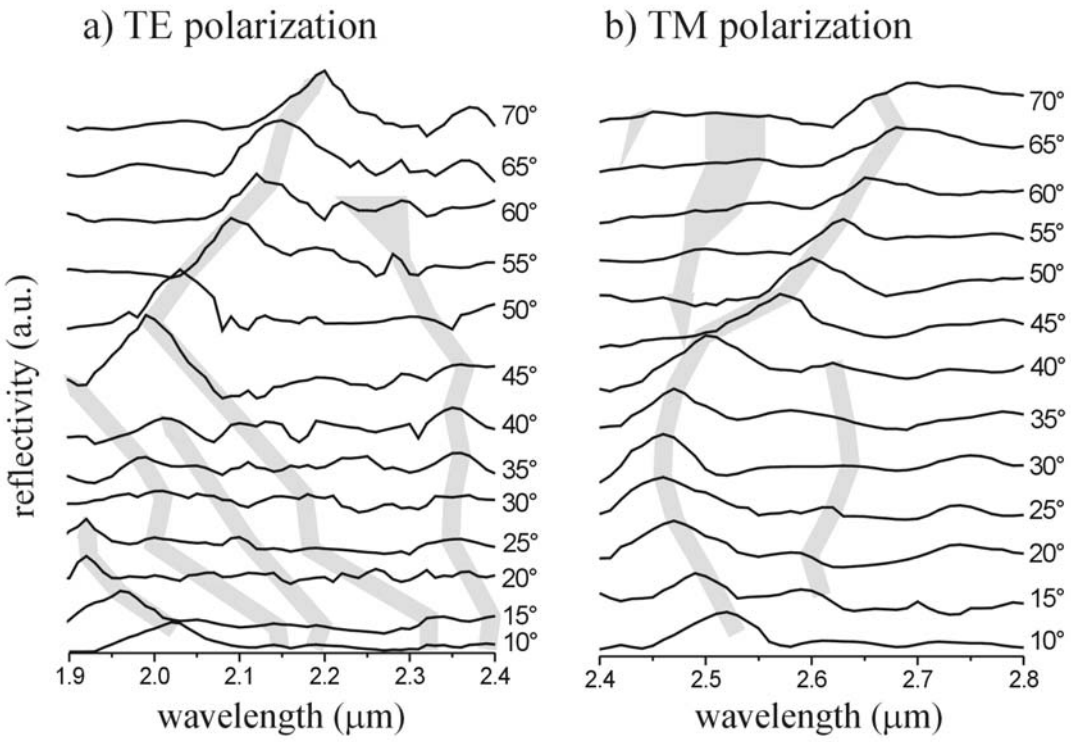

Reflectivity of the photonic crystal slab as a function of wavelength (black curves), measured along the Γ-M symmetry direction, a, for TE polarized and b, for TM polarized light. The curves are vertically shifted for clarity; from bottom to top, the angle of incidence increases from $\theta = 10°$ to 70°. The gray lines indicate reflectivity features.

Figure 5

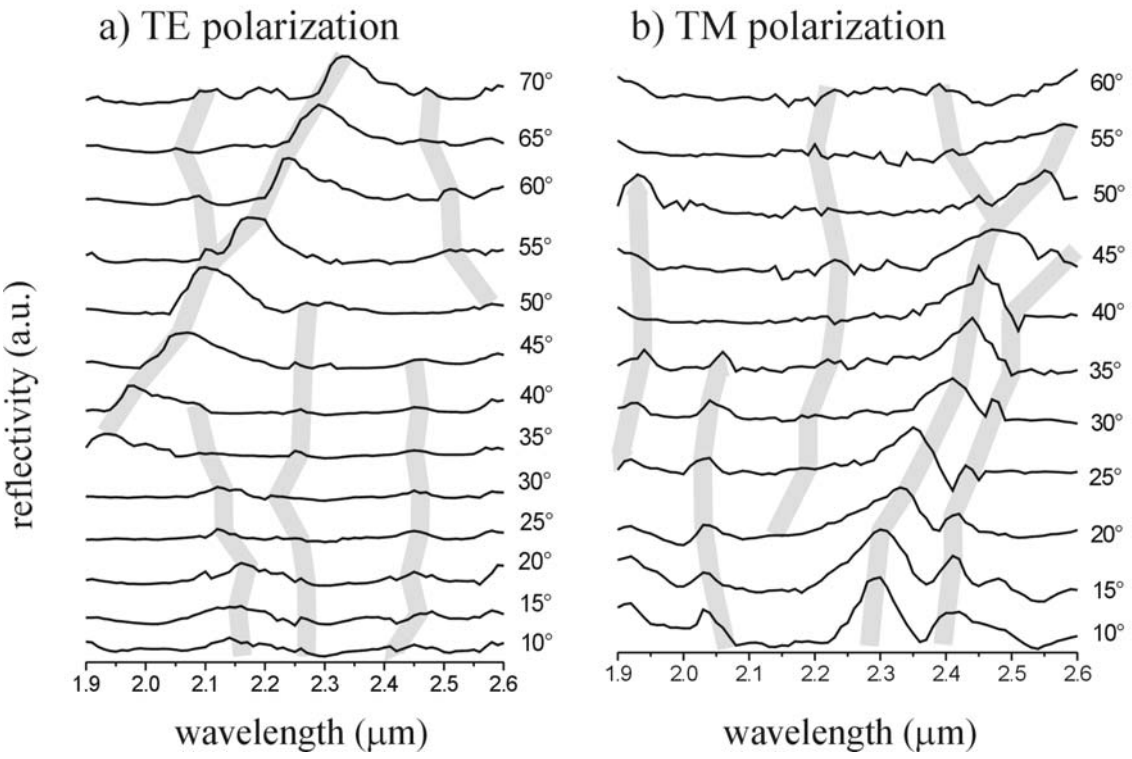

Reflectivity of the photonic crystal slab as a function of wavelength (black curves), measured along the Γ-X symmetry direction, a, for TE polarized and b, for TM polarized light. The curves are vertically shifted for clarity; from bottom to top, the angle of incidence increases from $\theta = 10°$ to 70° (a) and from 10° to 60° (b). The gray lines indicate reflectivity features.

Figure 6

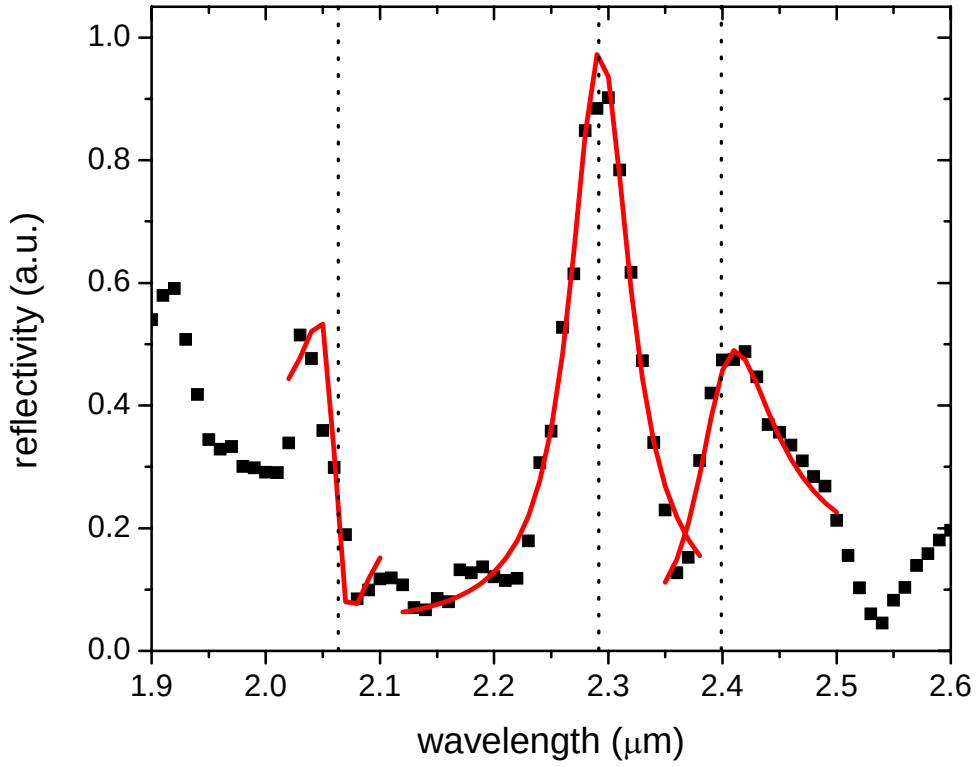

Example of a measured reflectivity spectrum with Fano-like line shapes. Squares: measured reflectivity for Γ–X symmetry direction, TM polarization, and 10° angle of incidence as a function of wavelength. Solid lines: Fano-line shapes fitted to three distinct reflectivity features. Dotted vertical lines: center wavelengths of the Fano line shapes.

Figure 7

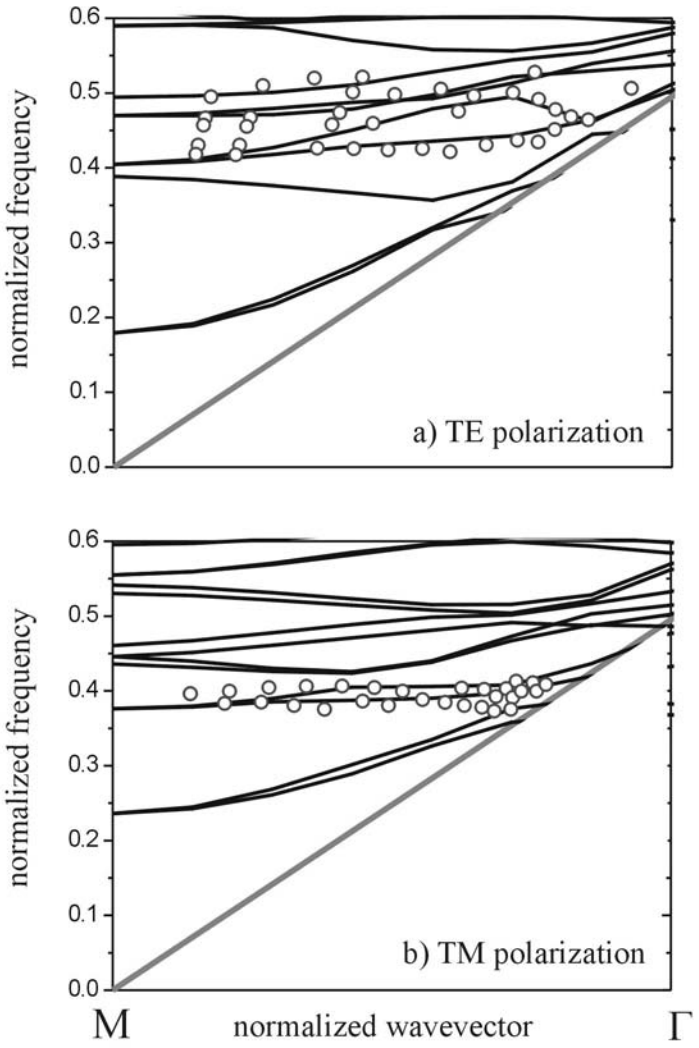

Out-of-plane band structure for Γ-M symmetry direction, a, for TE polarized light and b, for TM polarized light. The graphs show the dispersion obtained from the reflectivity experiments (open circles) together with calculated dispersion curves of the leaky modes (solid lines) above the light line, i.e. the dispersion of light in air (gray line).

Figure 8

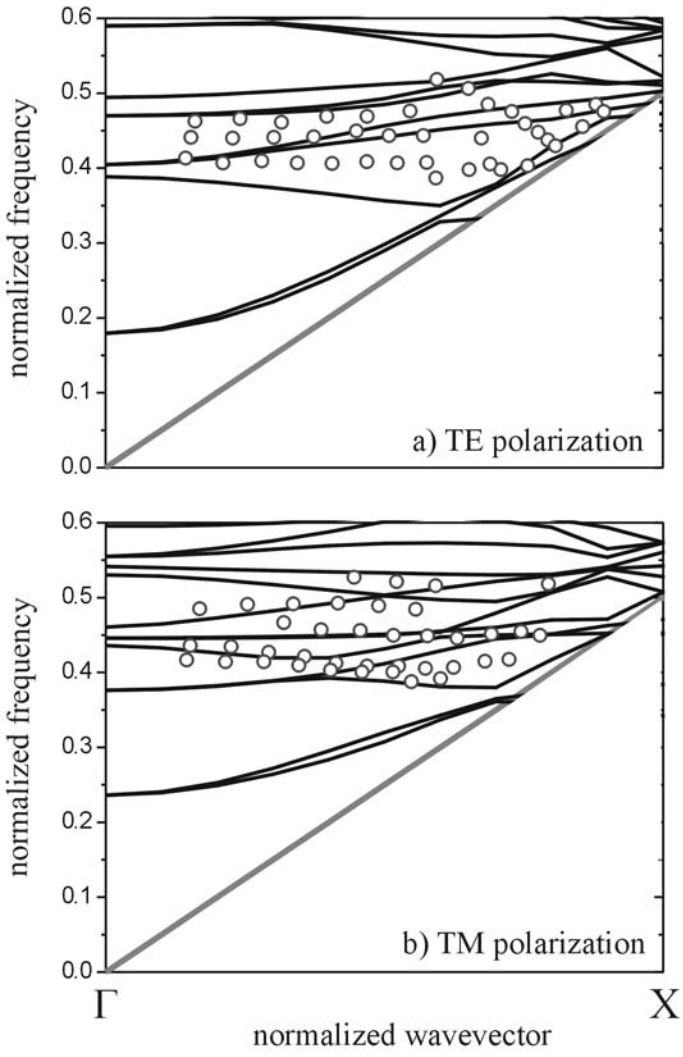

Out-of-plane band structure for Γ-X symmetry direction, a, for TE polarized light and b, for TM polarized light. The graphs show the dispersion obtained from the reflectivity experiments (open circles) together with calculated dispersion curves of the leaky modes (solid lines) above the light line, i.e. the dispersion of light in air (gray line).

Figure 9

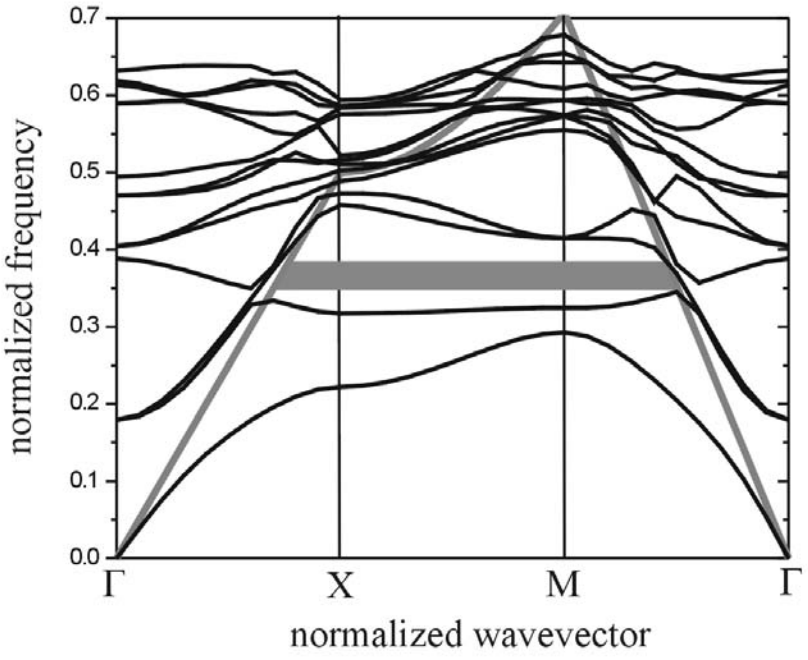

Calculated complete band structure for TE polarized light. Leaky and guided modes (solid black lines) are plotted above and under the light line (solid gray line), respectively. The guided modes exhibit a bandgap for normalized frequencies around 0.37 (gray bar).

Figure 10

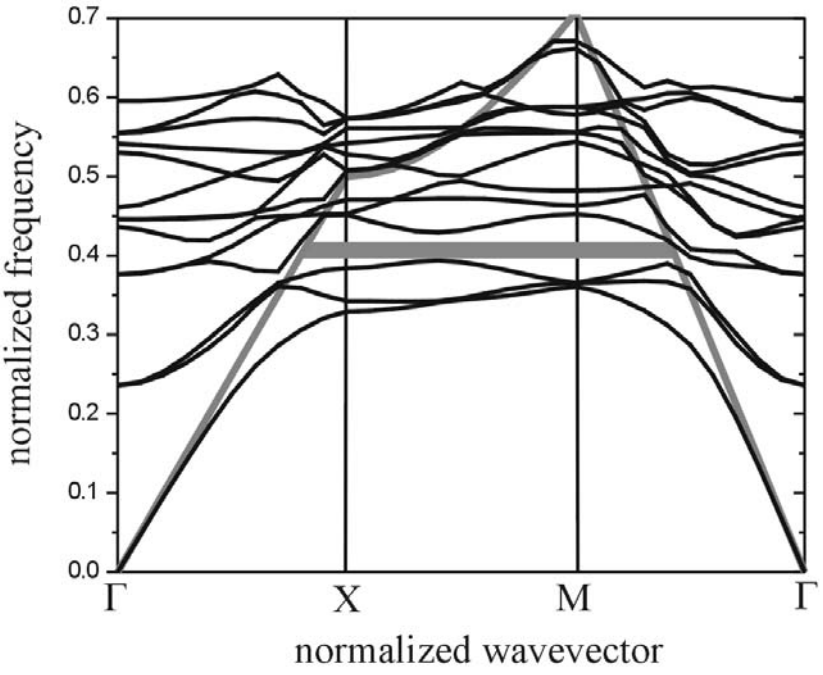

Calculated complete band structure for TM polarized light. Leaky and guided modes (solid black lines) are plotted above and under the light line (solid gray line), respectively. The guided modes exhibit a bandgap for normalized frequencies around 0.41 (gray bar).